Journal Name

ARTICLE TYPE

Cite this: DOI: 10.1039/xxxxxxxxxx

Received Date
Accepted Date

DOI: 10.1039/xxxxxxxxxx

www.rsc.org/journalname

Driving water cavitation into a hydrogel cavity†

Michele Curatolo,[a‡] Paola Nardinocchi*[b‡] and Luciano Teresi[a‡]

We study the dynamics of the dehydration process of a hydrogel with a cavity filled with water. We identify two transient phases: the first one dominated by an *inflatable-balloon* deformation mode, and the second by a *suction effect*, determining highly not homogeneous deformation modes of the hydrogel walls. This last phase triggers negative pressures into the cavity up to the typical values of water cavitation. An analysis of the factors allowing to get cavitation pressure inside the cavity is proposed, to allow for precise tuning of the key geometrical and material parameters.

1 Introduction

Cavitation is the phase transition liquid-to-vapor which happens in water under negative pressure, that is, under tension, and at constant ambient temperature; it has been firstly studied, as of great interest, in some industrial contexts such as marine propellers[1], and petroleum[2] industry. In the last years, cavitation occurring in microscopic confinement has received great attention, being one of the processes exploited in nature to realize shooting mechanisms used for prey capture, defense, and reproduction[3–5]. We only cite Ref. 3, and references therein, dealing with the dynamics of spontaneous or triggered cavitation inside water-filled micro-cavities of a hydrogel, where the stability of water under tension has been tested in experiments at constant tension and controlled humidity. Water-filled micro-cavities are the elementary units of fern sporangium which uses the cavitation induced by evaporation of the water to realize the shooting mechanism allowing for seeds dispersal. This shooting mechanism, described and discussed in Ref. 4, is composed of two phases: a slow opening phase driven by water evaporation which ends when cavitation pressure is attained within the micro-cavities; a fast closing phase triggered by water cavitation. The dynamics of the fern sporangium has been deeply studied, following optically the opening and closing of sporangia, computing the deformations of the annulus during the two phases, and interpreting the dynamics in terms of a one-dimensional beam model which is shown to finely capture the characteristics of the motion.

Results in Ref. 6 highlight the importance of the precise tuning of the parameters without which the function of the leptosporangium as a catapult would be severely compromised. Likewise, it is important to discuss and investigate through appropriate models the role of the key geometrical and material parameters allowing for the attainment of cavitation pressure in water-filled micro-cavities of a hydrogel. To do it, the de-hydration process of a hydrogel cavity, initially filled with water, exposed to air has to be modeled. The model has to take into account the pumping induced by the difference in chemical potential inside and outside the cavity, as well as the suction effect realized by the cavity walls during the evaporation phase. Some of the Authors have been involved in the investigation of hydration and dehydration processes in hydrogels for many years, and have elaborated a multiphysics model to describe such phenomena from a dynamics point of view which has been successfully tested in different situations[7–9].

Here, we deal with the following model experiment: a free-swollen hydrogel, having a cavity filled with water, is pulled out from the bath and exposed to air. The difference in chemical potential drains the water out of both cavity and gel walls, and a drying process begins. We study the dynamics of the dehydration process, identifying a transient phase dominated by an *inflatable-balloon* deformation mode, followed by a phase dominated by a *suction effect*, which determines highly not homogeneous deformation modes of the hydrogel. This phase triggers negative pressures into the cavity up to the typical values of water cavitation. This latter strongly depends on the geometry of the cavity, as well as on the shear modulus of the hydrogel. An analysis of the factors allowing to get cavitation pressure inside the cavity is proposed, to allow for precise tuning of the key geometrical and material parameters.

2 Theoretical Background

Our starting point is the multiphysics model presented and discussed in Ref. 7 and successively refined in Ref. 8 and Ref. 10, where the buckling dynamics of a solvent–stimulated and

[a] *Università degli Studi Roma Tre, via della Vasca Navale 84, Roma, Italy. E-mail: michele.curatolo@uniroma3.it, teresi@uniroma3.it*

[b] *Sapienza Università di Roma, via Eudossiana 18, Roma, Italy. Tel: +39 06 44 58 52 42; E-mail: paola.nardinocchi@uniroma1.it*

∗ *Corresponding author*

‡ These authors contributed equally to this work

stretched elastomeric sheet are investigated. The physical processes associated with swelling and de–swelling are described within the limits of a nonlinear field theory which views the water–polymer mixture as a homogenized continuum body, allowing for a mass flux of the solvent[11–14]. The mathematical modeling is derived from basic principles: the principle of null working and the conservation of the water mass deliver the balance equations of forces and solvent concentration, respectively; the dissipation principle select the admissible constitutive processes.

2.1 State variables and free energy

We introduce a *dry-reference state* $\mathscr{B}_d$ of the gel, and denote with $X_d \in \mathscr{B}_d$ a material point and with $t \in \mathscr{T}$ an instant of the time interval $\mathscr{T}$; we use the notation $[\alpha]$ to indicate the IS units of a quantity α. Our multiphysics model of gel has two state variables: the displacement field $\mathbf{u}_d(X_d,t)$ ($[\mathbf{u}_d]$=m), which gives the actual position $x = X_d + \mathbf{u}_d(X_d,t)$ of the point X_d at time t, and the molar water-concentration per unit dry volume $c_d(X_d,t)$ ($[c_d]$ =mol/m^3). A key point of this model is the volumetric constraint coupling these two state-variables:

$$J_d = \det \mathbf{F}_d = \hat{J}_d(c_d) = 1 + \Omega c_d \,, \tag{2.1}$$

where $\mathbf{F}_d = \mathbf{I} + \nabla \mathbf{u}_d$ is the deformation gradient and Ω is the molar volume of the water ($[\Omega]$ = m^3/mol). The constraint (2.1) implies that any change in volume of the gel is accompanied by an equivalent uptake or release of water content.

We consider a relaxed version of the Flory–Rehner thermodynamic model[15,16]; the free energy ψ per unit dry-volume is assumed to depend on $\mathbf{F}_d$ through an elastic component ψ_e, and on c_d through a polymer–water mixing energy ψ_m: $\psi = \psi_e + \psi_m$. The relaxed free–energy ψ_r, which includes the volumetric constraint, is written as:

$$\psi_r(\mathbf{F}_d, c_d, p) = \psi_e(\mathbf{F}_d) + \psi_m(c_d) - p(J_d - \hat{J}_d(c_d)) \,. \tag{2.2}$$

The pressure p represents the reaction to the volumetric constraint, which maintains the volume change J_d due to the displacement equal to the one due to solvent absorption or release $\hat{J}_d(c_d)$. Key features of ψ (or ψ_r) are the following: the elastic contribution ψ_e hampers swelling; the mixing contribution ψ_m favors swelling.

2.2 Stress and chemical potential

The constitutive equation for the stress $\mathbf{S}_d$ ($[\mathbf{S}_d]$=Pa = J/m^3) at the dry configuration $\mathscr{B}_d$, henceforth termed dry-reference stress, and for the chemical potential μ ($[\mu]$=J/mol) are derived from (2.2), which yields

$$\mathbf{S}_d = \hat{\mathbf{S}}_d(\mathbf{F}_d) - p\,\mathbf{F}_d^{\star} \quad \text{and} \quad \mu = \hat{\mu}(c_d) + p\,\Omega \,, \tag{2.3}$$

with

$$\hat{\mathbf{S}}_d(\mathbf{F}_d) = \frac{\partial \psi_e}{\partial \mathbf{F}_d} \,, \quad \hat{\mu}(c_d) = \frac{\partial \psi_m}{\partial c_d} \,, \quad \text{and} \quad \mathbf{F}_d^{\star} = J_d\,\mathbf{F}_d^{-T} \,. \tag{2.4}$$

Typically, the Flory–Rehner thermodynamic model prescribes a neo-Hookean elastic energy ψ_e and a polymer–water mixing energy ψ_m:

$$\psi_e(\mathbf{F}_d) = \frac{G_d}{2}(\mathbf{F}_d \cdot \mathbf{F}_d - 3) \,, \quad \psi_m(c_d) = \frac{\mathscr{R}T}{\Omega}\, h(c_d) \,, \tag{2.5}$$

with

$$h(c_d) = \Omega c_d \log \frac{\Omega c_d}{1+\Omega c_d} + \chi\, \frac{\Omega c_d}{1+\Omega c_d} \,, \quad [h] = 1 \,, \tag{2.6}$$

G being the shear modulus of the dry polymer, $\mathscr{R}$ the universal gas constant, T the temperature, and χ the Flory parameter. Their physical units are $[G]$=J/m^3, $[\mathscr{R}]$ =J/(K mol), $[T]$ = K. The dimensionless Flory parameter χ, called dis-affinity, is specific of each water–polymer pair. The parameter χ may possibly depend on temperature and deformation; these dependence are important when temperature–driven volume transition in hydrogels is studied, as in Refs. 17–19. Using (2.4), we can obtain the constitutive equations specific to our energy choice (2.5):

$$\begin{aligned} &\hat{\mathbf{S}}_d(\mathbf{F}_d) = G_d\,\mathbf{F}_d \,, \\ &\hat{\mu}(c_d) = \hat{\mu}(J_d) = \mathscr{R}T\left(\log\frac{J_d-1}{J_d} + \frac{1}{J_d} + \frac{\chi}{J_d^2}\right) , \end{aligned} \tag{2.7}$$

where, with a light abuse of notation, we wrote the relation for the chemical potential $\mu = \hat{\mu}(c_d)$ in terms of J_d as $\hat{\mu}(J_d)$ by exploiting the volumetric constraint (2.1). The actual stress (Cauchy) $\mathbf{T}$ is then given by the constitutive term $\hat{\mathbf{T}}(\mathbf{F}_d)$ minus the pressure term

$$\mathbf{T} = J_d^{-1}\mathbf{S}_d\,\mathbf{F}_d^T = \hat{\mathbf{T}}(\mathbf{F}_d) - p\,\mathbf{I} \,, \tag{2.8}$$

with $\hat{\mathbf{T}}(\mathbf{F}_d) = G_d/J_d\,\mathbf{B}_d$, and $\mathbf{B}_d = \mathbf{F}_d\,\mathbf{F}_d^T$.

2.3 Solvent flux

A key element in the transient swelling and de–swelling processes is the solvent flux. We assume the following prescription for the reference solvent flux $\mathbf{h}_d$, $[\mathbf{h}_d]$=mol/(m^2 s),

$$\mathbf{h}_d = \mathbf{h}_d(\mathbf{F}_d, c_d, p) = -\mathbf{M}(\mathbf{F}_d, c_d)\nabla(\hat{\mu}(c_d) + p\,\Omega) \,, \tag{2.9}$$

which is consistent with the dissipation principle, provided that the mobility tensor $\mathbf{M}(\mathbf{F}_d, c_d)$ is positive definite ($[\mathbf{M}]$=mol^2/(s m J)). Among the many admissible representations for the mobility, we assume $\mathbf{M}$ to be isotropic, and diffusion always to remain isotropic during any process. This is a largely shared assumptions (see Refs. 11,13,14, and Ref. 7 for a full discussion on the representations of $\mathbf{M}$ different from the isotropic one), and linearly dependent on c_d. We have:

$$\mathbf{M}(\mathbf{F}_d, c_d) = \frac{D}{\mathscr{R}T}\, c_d \mathbf{C}_d^{-1} \,, \quad \mathbf{C}_d = \mathbf{F}_d^T\mathbf{F}_d \,, \tag{2.10}$$

with D ($[D]$=m^2/s) the diffusivity. Using $\mathbf{m}$ to denote the outward unit normal, $q_s = -\mathbf{h}_d \cdot \mathbf{m}$ represents a boundary source of solvent, $[q_s]$=mol/(m^2 s). Hence, $q_s > 0$ corresponds to a positive source, that is, an inward flux.

2.4 The Initial-Boundary Value problem

The model is based on a system of bulk equations, describing the balance of forces and the balance of water concentration, coupled through the volumetric constraint (2.1), and the constitutive equations (2.3)-(2.6): on $\mathscr{B}_d \times \mathscr{T}$

$$0 = \mathtt{div}\, \mathbf{S}_d \quad \text{and} \quad \dot{c}_d = -\mathtt{div}\, \mathbf{h}_d\,, \tag{2.11}$$

with a dot denoting the time derivative and $\mathtt{div}$ the divergence operator. Equations (2.11) must be complemented with boundary conditions on the traction $\mathbf{t}$ and/or displacement $\bar{\mathbf{u}}_d$:

$$\mathbf{S}_d\,\mathbf{m} = \mathbf{t}\,, \text{on } \partial_t \mathscr{B}_d \times \mathscr{T}\,, \quad \mathbf{u}_d = \bar{\mathbf{u}}_d\,, \text{on } \partial_u \mathscr{B}_d \times \mathscr{T}\,; \tag{2.12}$$

and with chemical boundary conditions on solvent source q_s and/or concentration $\bar{c}_d$:

$$\begin{aligned} -\mathbf{h}_d \cdot \mathbf{m} &= q_s\,, \qquad \text{on } \partial_q \mathscr{B}_d \times \mathscr{T}\,, \\ \hat{\mu}(\bar{c}_d) + p\,\Omega &= \mu_{ext}\,, \text{ on } \partial_c \mathscr{B}_d \times \mathscr{T}\,. \end{aligned} \tag{2.13}$$

We note that the boundary concentration $\bar{c}_d$ is assigned implicitly by controlling the external chemical potential μ_{ext}.

Notation $\partial_s \mathscr{B}_d$ with $s = t, u, q$ or c in the above equations refers to the portion of the boundary of $\mathscr{B}_d$ where traction $\mathbf{t}$, displacement $\bar{\mathbf{u}}_d$, solvent source q_s, and concentration $\bar{c}_d$ are prescribed, respectively. Finally, the model is completed by the initial conditions for the state variables $\mathbf{u}_d$ and c_d:

$$\mathbf{u}_d = \mathbf{u}_{do}\,,\ c_d = c_{do}\,, \quad \text{on } \mathscr{B}_d \times \{0\} \tag{2.14}$$

3 Drying–driven suction effect

The time–dependent stress–diffusion problem described above allows to investigate both hydration and dehydration, which cause swelling and de–swelling, respectively. The latter process has received little attention in the Literature, even if it can induce noteworthy phenomena as the one we are studying here. Let us start by considering an ideal experiment. A dry hydrogel $\mathscr{B}_d$, with an inner cavity $\mathscr{C}_d$, is immersed into a water bath in absence of constraints and loads, and kept there until both the hydrogel walls and the cavity are completely filled with water* At this point, the hydrogel is in a steady, stress-free state $\mathscr{B}_o$, with cavity $\mathscr{C}_o$; it is then taken out of the bath and exposed to air: dehydration begins, and water is expelled from both the cavity and the gel walls (figure 1).

* We can imagine cube, with a cubic cavity, and a cut open face; the cube is immersed into a bath until it is fully swollen. Then, the cut is sealed, and the swollen cube, with its cavity filled with water is put in open air and let dehydrate.

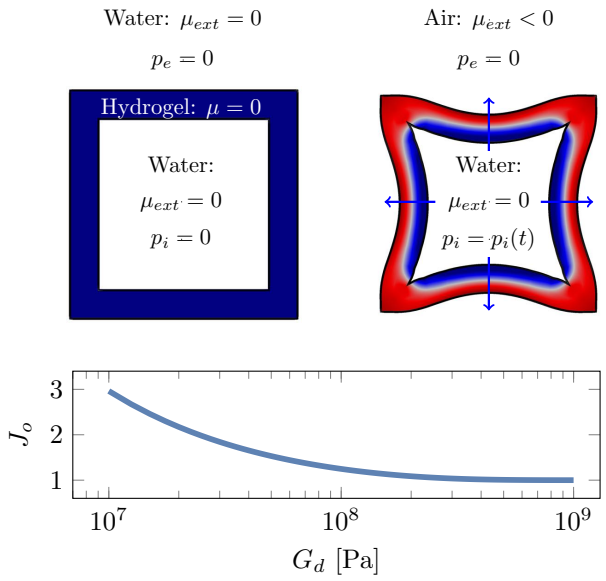

Fig. 1 Top: A hydrogel cube with a cavity sits into a bath, in a free-swollen, steady state; the cavity is completely filled with water (left). The same hydrogel is pulled out and exposed to air: dehydration begins and water is pumped out of the cavity by the difference in chemical potential. As water content of the cavity reduces, the walls experience a suction pressure which yields an inward bending (right). Bottom: Free-swelling volume J_o versus shear modulus G_d for an external chemical potential $\mu_{\text{ext}} = 0$ J/mol (see Table 1 for parameters value).

3.1 Modeling Dehydration

Here, we are interested in the dynamics of the dehydration process, that is, in describing the actual configuration of the gel $\mathscr{B}_\tau$, and of its cavity $\mathscr{C}_\tau$, during the time evolution:

$$\underbrace{\mathscr{B}_d\,, \mathscr{C}_d}_{\text{dry-reference state}} \quad \rightarrow \quad \underbrace{\mathscr{B}_o\,, \mathscr{C}_o}_{\text{free-swollen state}} \quad \rightarrow \quad \underbrace{\mathscr{B}_\tau\,, \mathscr{C}_\tau}_{\text{dehydration dynamics}} \tag{3.15}$$

As well described in Literature (see Refs. 4–6), the volume of the cavity has to match the volume of the water it contains: as water is pumped out, the volume of the cavity reduces, a suction pressure develops, and the hydrogel walls slowly bend inward. Correspondingly, elastic energy is stored into the walls. The suction effect, due to the water incompressibility, yields a negative pressure in the water, that is, a tension; eventually, if water tension reaches a critical value (in the range minus $9 \sim 20$ MPa) relative to the ambient pressure, cavitation can occurs: the formation of vapor bubbles in the cavity suddenly increases the volume occupied by water, yielding a jump of the suction pressure: hydrogel walls quickly release all the elastic energy previously stored. This whole process can be viewed as a power amplifier: chemical energy is used to slowly increase the elastic energy of the gel, a low-power process; then, this elastic energy is rapidly converted in kinetic energy and dissipated, a high-power process. This point of view has been illustrated in Ref. 4 and largely reviewed in Ref. 5; water cavitation is the breaking factor that switches the slow process to the fast one.

Being interested in dehydration, we consider as initial configuration the swollen, stress-free, steady state $\mathscr{B}_o$: with zero loads,

no constraints, and an external chemical potential $\mu_{ext} = \mu_o$, the mechanical and chemical balance laws prescribe $\mathbf{S}_d = \mathbf{0}$, $\mu = \mu_o$, and yield a uniform deformation $\mathbf{F}_d = \mathbf{F}_o = \lambda_o \mathbf{I}$. The stretch λ_o is characterized by the value μ_o of the bath's chemical potential: the zero-stress condition yields the pressure p

$$\mathbf{S}_d = G_d \mathbf{F}_o - p\,\mathbf{F}_o^\star = \mathbf{0} \quad \Rightarrow \quad p = \frac{G_d}{\lambda_o}\,. \tag{3.16}$$

By substituting p in the constitutive relation for the chemical potential yields a non linear equation relating μ_o and λ_o

$$\hat{\mu}(J_o) + \frac{G_d}{\lambda_o}\,\Omega = \mu_o\,, \quad \text{with} \quad J_o = \lambda_o^3. \tag{3.17}$$

The relationship between J_o and G given by the equation (3.17) is represented for $\mu_o = 0$ in figure 1 (bottom); it shows as the initial conditions change, depending on the shear modulus of the hydrogel, once all the other parameters have held fixed. Equation (3.17) is also used to set the initial conditions (2.14) specific to our problem†:

$$\mathbf{u}_o = (\lambda_o - 1)\,x\,, \quad c_d = c_{do} = \frac{J_o - 1}{\Omega}\,, \quad \text{on } \mathscr{B}_\mathrm{d} \times \{0\}\,. \tag{3.18}$$

The deformation from $\mathscr{B}_o$ to the actual state $\mathscr{B}_t$ is then described by the deformation gradient $\mathbf{F} = \mathbf{F}_d\,\mathbf{F}_o^{-1}$. As regards mechanical boundary conditions, we consider a steady uniform pressure p_e on the external boundary $\partial_e \mathscr{B}_d$, and a time-varying pressure p_i on the internal boundary $\partial_i \mathscr{B}_d = \partial \mathscr{C}_d$, with $\partial \mathscr{C}_d$ the boundary of the cavity; in terms of reference stress, we have

$$\begin{aligned} \mathbf{S}_d\,\mathbf{m} &= -p_e\,\mathbf{F}_d^\star\,\mathbf{m}\,, \text{ on } \partial_e \mathscr{B}_d \times \mathscr{T}\,, \\ \mathbf{S}_d\,\mathbf{m} &= -p_i\,\mathbf{F}_d^\star\,\mathbf{m}\,, \text{ on } \partial \mathscr{C}_d \times \mathscr{T}\,. \end{aligned} \tag{3.19}$$

The external pressure p_e describes the effect of the atmospheric pressure, and we assume as base value $p_e = 0$ Pa. The internal pressure $p_i = p_i(t)$ is a key element in our problem, and arises as reaction to the volumetric coupling between the water volume $v_w = v_w(t)$, and the cavity volume $v_c = v_c(t)$. As water flows out of the cavity it must hold

$$v_c(t) = v_w(t) \tag{3.20}$$

at each instant $t \in \mathscr{T}$. The global constraint (3.20) is enforced by adding a term to the total relaxed free-energy ψ_r:

$$\text{Potential Energy} = \int_{\mathscr{B}_d} \psi_r\,dV - p_i\,(v_c - v_w)\,; \tag{3.21}$$

thus, p_i can be viewed as the Lagrange multiplier enforcing the constraint (3.20). The cavity volume v_c depends on the actual configuration of the gel, described by the displacement $\mathbf{u}_d$, and can be evaluated as

$$v_c(t) = \int_{\mathscr{C}_t} dv = \frac{1}{3}\int_{\partial \mathscr{C}_t} x \cdot \mathbf{n}\,da = \frac{1}{3}\int_{\partial \mathscr{C}_d} (X_d + \mathbf{u}_d)\cdot \mathbf{F}_d^\star\,\mathbf{m}\,dA_d\,. \tag{3.22}$$

† The initial condition for $\mathbf{u}_d$ assumes that the cubic region $\mathscr{B}_d$ is centered at the origin.

On the other hand, the water volume v_w equals the initial water content v_{wo}, minus the volume $v_w^i(t)$ of water outflown through the inner boundary, that is, that has left the cavity during the time interval $(0,t)$:

$$v_w(t) = v_{wo} - v_w^i(t)\,. \tag{3.23}$$

The initial water content equals the initial cavity volume $v_{co} = v_c(0)$, and is given by (3.22), evaluated at time $t = 0$:

$$v_{wo} = v_{co} = v_c(0) = \frac{1}{3}\int_{\partial \mathscr{C}_d} (X_d + \mathbf{u}_o)\cdot \mathbf{F}_o^\star\,\mathbf{m}\,dA_d\,. \tag{3.24}$$

To evaluate the volume v_w^i of the water that has left the cavity, we have at our disposal its time-rate $\dot{v}_w^i$ as $q_s = -\mathbf{h}_d \cdot \mathbf{m}$ measures the water flux entering the gel through the boundary. It follows

$$\dot{v}_w^i(t) = \int_{\partial \mathscr{C}_d} q_s\,dA_d = -\int_{\partial \mathscr{C}_d} \mathbf{h}_d \cdot \mathbf{m}\,dA_d\,. \tag{3.25}$$

Eventually, by time-integrating $\dot{v}_w^i(t)$, with initial condition $v_w^i(0) = 0$, yields the function $v_w^i(t)$. It is worth noting that both v_c and v_w depend on the state of the gel, that is, on the two state variables $\mathbf{u}_d$, c_d, which were coupled as a consequence of (2.1). Hence, the new global constraint (3.20) adds a further coupling, through the inner pressure p_i.

As regards the chemical boundary conditions, we use different values for the external chemical potential μ_ext, at the inner and the outer boundary of the gel:

$$\mu_\mathrm{ext} = \mu_w \text{ on } \partial \mathscr{C}_d\,, \quad \text{and} \quad \mu_\mathrm{ext} = \mu_a \text{ on } \partial_e \mathscr{B}_d\,, \tag{3.26}$$

being $\mu_w = 0$ J/mol a constant value at the surface in contact with water, and $\mu_a = \mu_a(t)$ a time varying value at the surface being exposed to air (see figure 1, top). To model the transient time interval during which the outer boundary condition changes from water to air, we assume the following time law for μ_a:

$$\mu_a(t) = \mu_o + (\mu_\infty - \mu_o)(1 - \texttt{exp}[-\texttt{log}2\,(t/T_c)])\,, \tag{3.27}$$

with $\mu_o = 0$ J/mol, corresponding to Relative Humidity (RH) equal to 1, and $\mu_\infty \ll \mu_o$, corresponding to RH $\ll 1$; T_c is the time needed to go from μ_o to $(\mu_o + \mu_\infty)/2$. In our numerical experiments we use the following values of the materials parameters:

Table 1 Numerical values of the parameters

Parameter value	IS Units	Description
$\Omega = 1.8 \cdot 10^{-5}$	m^3/mol	water molar volume;
$\chi = 0.2$	1	dis-affinity;
$D = 10^{-9}$	m^2/s	diffusivity;
$\mu_\infty = -2000$	J/mol	chemical potential for air ($J_\infty \simeq 1$);
$Tc = 500$	s	time to switch wet-to-dry;
$T = 293$	K	ambient temperature.

4 Dehydration dynamics

We consider as dry-reference $\mathscr{B}_d$ a cube with side length l, having a cubic cavity $\mathscr{C}_d$ at its center with side length $l - h$, so that the gel walls have thickness $h/2$.

4.1 Early dynamics

To discuss dehydration dynamics we introduce the following volume ratios, whose time behavior is shown in figure 2:

- $v_w^i(t)/v_{co}$ water through the inner boundary;
- $v_w^e(t)/v_{co}$ water through the external boundary;
- $v_g(t)/v_{co}$ gel volume: $v_g = \int_{\mathscr{B}_d} J_d \, dV$;
- $v_w(t)/v_{co}$ water content of the cavity.

We also remember that water flux is measured with respect to the gel, that is, positive values of v_w^i and v_w^e represent water entering the gel.

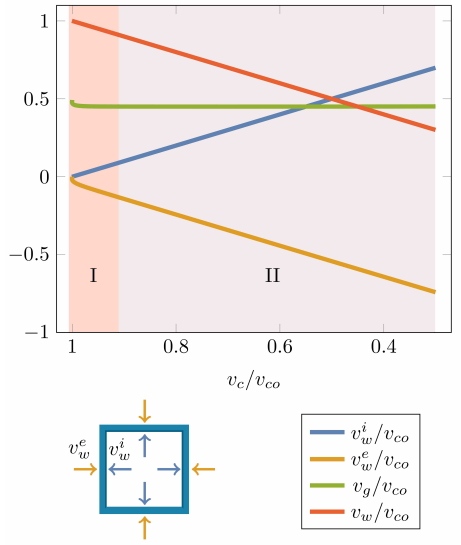

Fig. 2 Top: Volume ratios of different quantities versus the dimensionless cavity volume v_c/v_{co}: volume of water crossing the internal boundary, v_w^i/v_{co} (blue); volume of water crossing external boundary v_w^e/v_{co} (yellow); gel volume v_g/v_{co} (green); water content of the cavity v_w/v_{co} (red). We set: $G_d = 10^8$Pa, $h = 0.0025$m, $l = 0.02$m; at $t = 0$, cavity volume is twice the gel volume.

Let $t_c = h^2/4D$ be the characteristic time of the diffusion problem. At early times, that is for $t/t_c << 1$, when hydrogel begins to release water from the external walls towards the environment, we have the highest gradients of chemical potential. The small, steep, ramp at the beginning of the curve $v_w^e(t)/v_{co}$ (yellow line) corresponds to a large negative flux (water exits from the walls); during the same time interval, the water entering the gel from the cavity is much smaller, $\|v_w^i(t)/v_{co}\| \ll \|v_w^e(t)/v_{co}\|$, the water content in the gel decreases very fast, and so does the gel volume, $v_g(t)/v_{co} < 1$ (steep initial ramp of the green line); meanwhile, the cavity volume remains almost unchanged, $v_w(t)/v_{co} \simeq 1$ (red line).

As a consequence, the inner pressure p_i increases up to a maximum positive value (figure 3, top panel), and we observe a sort of inflatable–balloon effect of the cavity which is especially visible under certain conditions, as we are discussing in the next subsection.

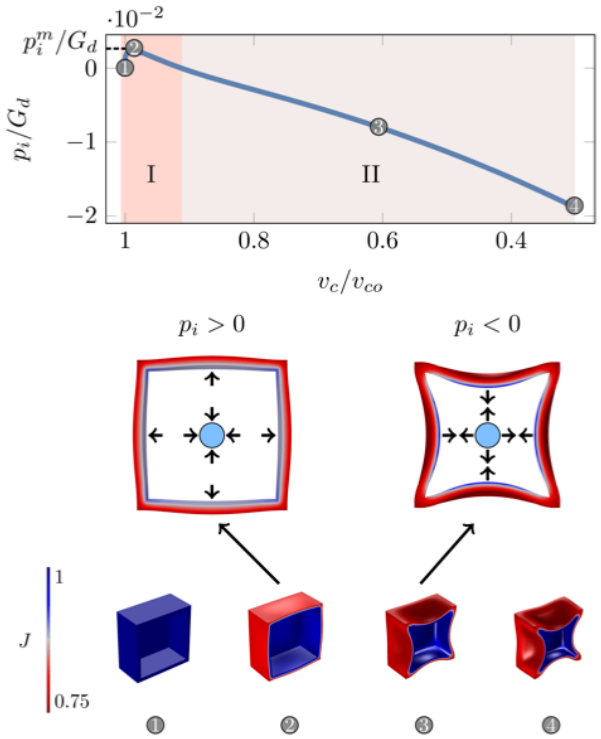

Fig. 3 Top: Dimensionless inner pressure p_i/G_d versus cavity volume v_c/v_{co}; cavity pressure changes sign from positive in phase I to negative in phase II. At point 2, the pressure has its maximum, denoted as p_i^m. Middle: Gel configurations under positive (left) and negative (right) inner pressure. Bottom: Gel configurations at the four points $1-2-3-4$ highlighted in the top plot; coloring according to the gel-volume variation J. We set: $G_d = 10^8$ Pa, $h = 0.0025$ m, $l = 0.02$ m.

The pink region in figure 2 and 3, labeled I, identifies this phase of the dehydration, characterized by a positive inner pressure p_i and the inflatable–balloon deformation mode. This mode is represented with a cartoon in figure 3 (bottom panel, left), where coloring corresponds to the value of $J = J_d/J_o$, the ratio between the current and the free-swollen volume of the hydrogel.

After this initial transient, when $t/t_c > 1$, the gel volume $v_g(t)/v_{co}$ remains almost constant, see green line in figure 2, as the water entering into the gel from the cavity (blue line) is equal to water exiting the gel from the external boundary (yellow line).

The gray region in figure 2 and 3, labeled II, identifies the second phase of the dehydration, during which the inner pressure p_i has negative values, thus yielding the suction effect. During this phase, the hydrogel walls bend inwards, and the water inside the cavity undergoes tension; this effect is represented with a cartoon in figure 3 (bottom panel, right).

4.2 Flow rates

A better view of the dehydration process can be obtained through the analysis of the fluxes and the pressure versus the cavity volume, as shown in figure 4; here phase I is larger than phase II, due to the smaller value of the shear modulus that has been used ($G_d = 10^7$ Pa) with respect to the one used for figure 3 to better discuss the process.

It can be noticed that the external flow rate $\dot{v}_w^e$ (yellow line)

begins with a very high negative value: a lot of water exits from the gel towards the external; at the same time, the internal flow rate $\dot{v}_w^i$ (blue line) has a much smaller negative value: few water exits from the gel towards the cavity. Pressure (green dashed line) is positive and the inflatable–balloon effect takes place; when the two flow rates approach the same absolute value, $\|\dot{v}_w^e\|/\|\dot{v}_w^i\| \to 1$, the inner pressure crosses the zero value and becomes negative: the suction effect begins.

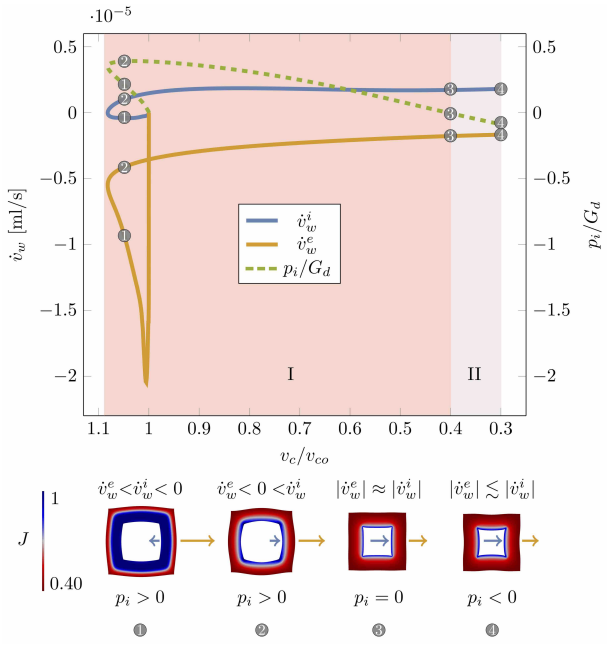

Fig. 4 Top: Flow rates $\dot{v}_w^i$ (blue, solid) and $\dot{v}_w^e$ (yellow, solid) of water crossing the cavity boundary, and the external boundary, respectively; values are reported on the left vertical axis. Dimensionless pressure p_i/G_d (green, dashed) inside the cavity; values are reported on the right vertical axis. Bottom: Gel configurations corresponding to the four points highlighted on the above plot. The arrows show flow rates; coloring according to the gel-volume variation J. We set: $G_d = 10^7$ Pa, $h = 0.0025$ m, $l = 0.005$ m.

The cartoon at the bottom of figure 4 shows four different configurations corresponding to the points reported in the above plot. Configuration 1: very early times; $\dot{v}_w^e < \dot{v}_w^i < 0$; hydrogel walls are releasing water towards both the external environment and the inner cavity; pressure is positive and inflation begins. Configuration 2: early times; $\dot{v}_w^e < 0 < \dot{v}_w^i$; water exits from the cavity and from the external boundary, while $p_i > 0$; inflation persists. Configuration 3: flow rate are almost equal, but opposite in sign: $\|\dot{v}_w^e\|/\|\dot{v}_w^i\| \to 1$; pressure is almost zero. Configuration 4: inward flow rate from the cavity remains slightly higher than the outward flow rate to the external environment; $|\dot{v}_w^i| \gtrsim |\dot{v}_w^e|$; pressure becomes negative; suction begins.

All in all, the flow rate from the cavity $\dot{v}_w^i$ depends on the geometrical characteristic of the cubic sample. In particular, our cube with edge length $= l$ and walls thickness $= h/2$, has external faces with area $A_e = l^2$, and cavity faces with area $A_c = (l-h)^2$; the ratio $a_\beta = A_e/A_c$ has a key role. Given the slenderness ratio $\beta = h/l$, it holds $a_\beta = 1/(1-\beta)^2$. We tested values for $\beta \in (1/8, 1/2)$, that is, from thin wall and large cavity ($\beta \sim 1/8$), to thick wall and small cavity ($\beta \sim 1/2$), yielding a_β in the range $(1.3, 4)$. As expected, see figure 5, $\dot{v}_w^i$ is a decreasing function of a_β and is lower for stiffer hydrogels (green lines) than for softer hydrogels (orange and blue lines); these values correspond to the instant $\bar{\tau}$ when, for each different sample, the cavity volume is half the initial size: $v_c(\bar{\tau})/v_{co} = 1/2$.

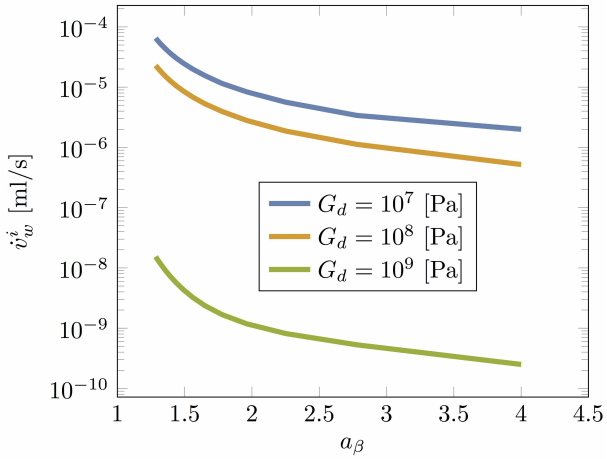

Fig. 5 Semi-log plot of the flow rate through the boundary of the cavity $\dot{v}_w^i$, evaluated when $v_c/v_{co} = 1/2$, versus the surface ratio a_β. The three curves refer to different shear moduli, ranging from $G_d = 10^7$ Pa to $G_d = 10^9$ Pa (semi–logarithmic scale).

4.3 Elastic energie and stress

Finally, we discuss the evolution of two mechanical quantities, the elastic energy and the stress state, by comparing the behavior of gels having different shear moduli.

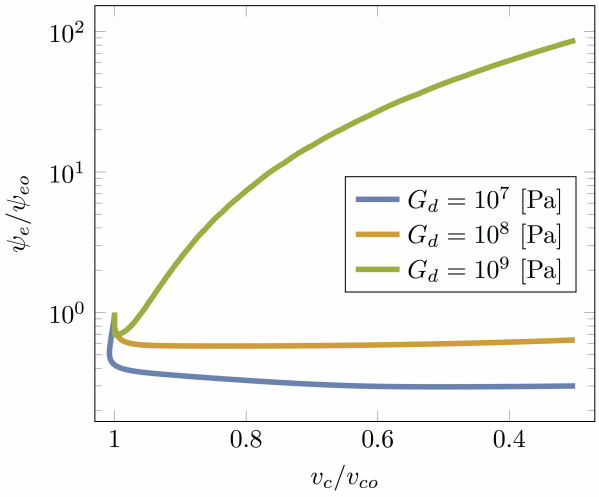

Fig. 6 Dimensionless elastic energy ψ_e/ψ_{eo} versus v_c/v_{co} for different shear moduli spanning three orders of magnitude. We set: $h = 0.0025$ m, $l = 0.02$ m.

During dehydration, a large part of elastic energy should be stored as a consequence of the suction–effect deformation mode,

that eventually yields a cavitation pressure inside the cavity[‡]. In figure 6 we plot the evolution of the dimensionless elastic energy ψ_e/ψ_{eo}, with ψ_{eo} the elastic energy stored at the free-swollen state. We observe that, for a stiff material (green lines), the function ψ_e/ψ_{eo} is not monotone: at early times elastic energy decreases; then, at later times, it increases much more with respect to the previous loss. For softer hydrogels, the elastic energy behaves differently (orange and blue lines): most of its change happens at early times, with the consequence that the change of elastic energy during the process is much smaller with respect to the one seen for stiff gels.

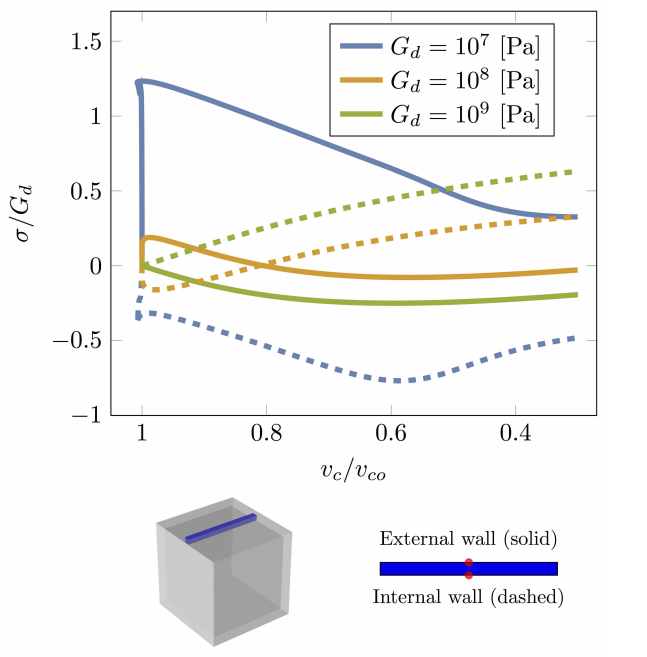

Fig. 7 Top: Dimensionless bending stresses σ/G_d versus v_c/v_{co} for different shear moduli. Values taken at the external side (solid lines), and the internal side (dashed lines) of the cross section. Bottom: cartoon of the cubic sample with the beam-like region highlighted in blue (left), and the points used to evaluate the stress in red (right). We set: $h = 0.0025$ m, $l = 0.02$ m.

To analyze the stress state, we focus on a beam-like portion of the gel's wall, that is, we consider a region at the center of a cube face, having length $(l-h)$ and cross section $h/2 \times h/2$ (see cartoon at bottom of figure 7). Denoted with $\mathbf{e}$ the direction of the longitudinal axis of the beam, we are interested in the longitudinal component of the stress $\sigma = \mathbf{T}\mathbf{e}\cdot\mathbf{e}$, which is the stress component important for the bending. In figure 7, we plot the evolution of the dimensionless stress σ/G_d evaluated at a point of the external wall (solid lines), and of the internal wall (dashed lines). The stress analysis is interesting for two reasons. Firstly, it shows as stiff hydrogels (green) have a stress distribution in accordance with the suction–effect mode (stress is negative at outside, and positive at inside), whereas soft gels (orange lines) presents an inversion of the bending couple when deformation mode switches from the inflation–balloon (positive at outside, and negative at inside) to the suction–effect (negative at outside and positive at inside). Even softer hydrogels (blue lines) only presents bending stresses compatible with the inflation–balloon mode. Moreover, in these latter softer hydrogels, bending stress attains a very high values at early times.

‡ In Ref. 4, it has been noted as an array of cells, each undergoing a suction–effect deformation mode, exhibits a global bending deformation.

4.4 The inflation–balloon effect

At the best of our knowledge, the inflatable–balloon mode observed at early times has never been noted in the Literature. This phenomenon strongly depends on G_d, χ, μ_∞, β and the ratio T_c/t_c; in particular, by controlling T_c, the inflation effect can be enhanced or diminished. To quantify the effect of T_c/t_c and G_d, we fixed the aspect ratio $\beta = 0.125$ of the cubic sample, the external chemical potential $\mu_\infty = -2000$ J/mol, and we studied the dependence of the maximum inner pressure p_i^m, made dimensionless by G_d (see point 2 in figure 3), on T_c/t_c and on G_d. It is worth noting that, being μ_o fixed, from equation (3.17) $J_o = J_o(G_d)$, see equation (3.17); thus, in the plot we report the values of J_o instead of G_d.

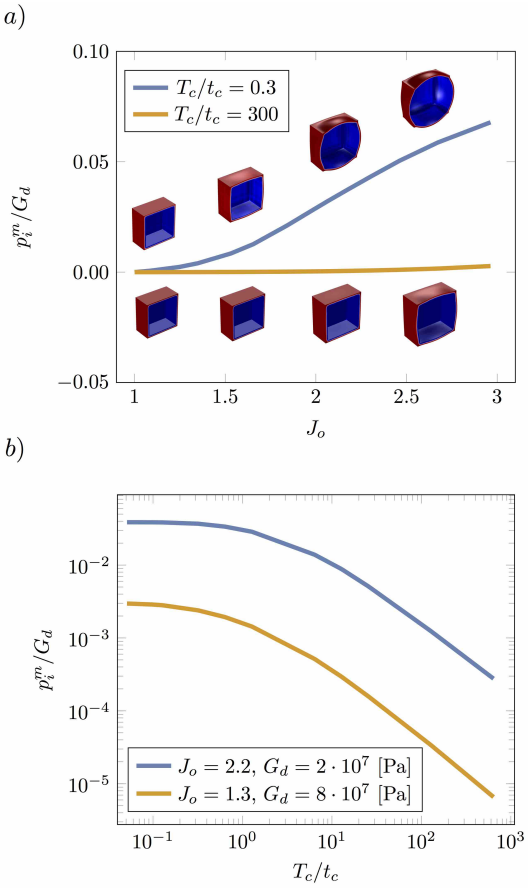

Fig. 8 Inflatable–balloon mode. Top: Maximum dimensionless pressure p_i^m/G_d versus J_o at different ratios T_c/t_c (panel a). Bottom: Log-log plot of maximum dimensionless pressure p_i^m/G_d versus T_c/t_c at different J_o (panel b). We remember that $J_o = J_o(G_d)$; thus to each value of J_o there correspond a unique value of G_d; see figure 1, bottom.

Figure 8a shows p_i^m/G_d versus J_o. The inflatable–balloon mode increases with J_o, and becomes appreciable when $J_o > 2$; moreover, the same effect is hampered for $T_c > t_c$ (yellow). Indeed, only when $T_c < t_c$ (blue), the water begins to outflow from the external boundary faster with respect to the water entering in the gel from the cavity: thus, the shrinking walls have to be stretched in order to wrap the water volume in the cavity which is still large. Figure 8b shows p_i^m/G_d versus T_c/t_c. The curves show two regimes: for $T_c/t_c \lesssim 2\cdot 10^{-1}$, pressure remains constant; for $T_c/t_c \gtrsim 2\cdot 10^1$ pressure decreases linearly (in a log-log plot). When $T_c/t_c > 10^2$, the maximum inner pressure is too low, and it is almost impossible to observe the inflatable-balloon mode. The dimensionless pressure p_i^m/G_d is higher for the softer gel (blue) than for stiffer ones (yellow); the same holds for the dimensional pressure p_i^m: at early times, $p_i^m \sim 6\cdot 10^5$ Pa for the soft gel, and $p_i^m \sim 1.6\cdot 10^5$ Pa for the stiff one.

5 Determinants for cavitation

We investigate how geometrical and material factors may trigger water cavitation, assuming $p_i = -10$ MPa as threshold for the phenomenon to happen. Through our numerical experiments, we discovered that shear modulus G_d, and slenderness parameter β are the main determinants in attaining cavitation.

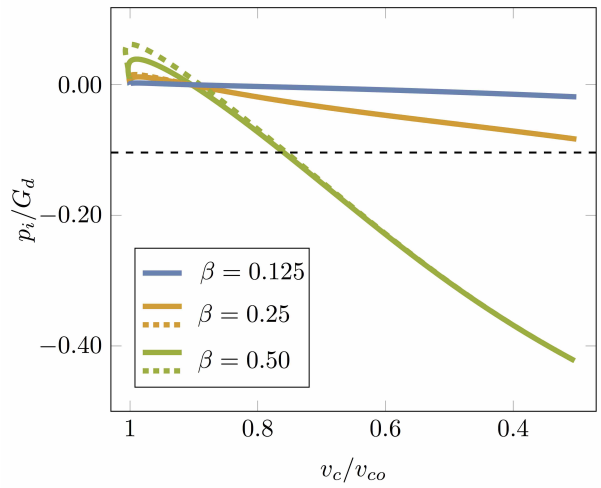

Fig. 9 Dimensionless inner pressure p_i/G_d versus v_c/v_{co}, for different values of β and fixed $G_d = 10^8$ Pa. Solid lines are obtained with $h = 0.0025$ m and $l = (0.02\,\text{m}, 0.01\,\text{m}, 0.005\,\text{m})$, corresponding to $\beta = (0.125, 0.25, 0.50)$, respectively (blue, orange and green solid lines). Dashed lines are obtained with $l = 0.02$ m and $h = (0.005\,\text{m}, 0.01\,\text{m})$, corresponding to $\beta = (0.25, 0.50)$, respectively (orange and green dashed lines). The black dashed line represents the dimensionless pressure of water cavitation $p_c/G_d = -0.1$, with $G_d = 10^8$ Pa.

At first, we investigate the dependence on β with a constant $G_d = 10^8$ Pa. Figure 9 shows dimensionless inner pressure p_i/G_d versus volume ratio v_c/v_{co}, for different values of β. We note that only the green curves, corresponding to $\beta = 0.5$ attain values below the dimensionless cavitation pressure (black, dashed). Cavitation should occur when the volume of the cavity has been reduced to about 70%. More slender sample, with shear modulus $G_d = 10^7$ Pa cannot achieve cavitation pressure.

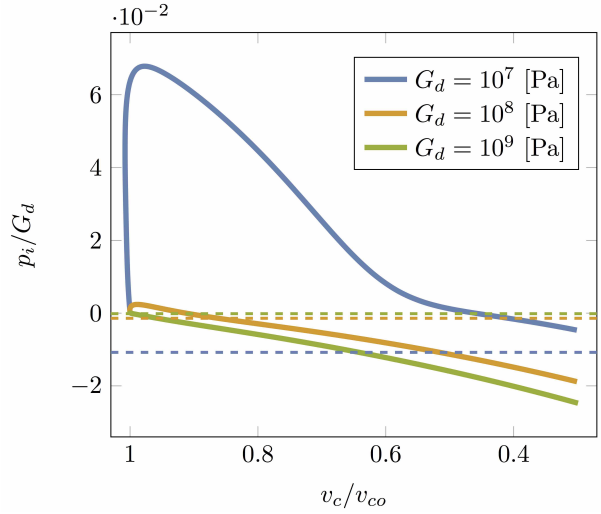

Fig. 10 Dimensionless inner pressure p_i/G_d versus v_c/v_{co} for different values of G_d (solid lines). Dashed lines correspond to the dimensionless cavitation pressure for $G_d = 10^7$ Pa (blue), $G_d = 10^8$ Pa (green), $G_d = 10^9$ Pa (orange). We set: $h = 0.0025$ m, $l = 0.02$ m.

Then, we investigate the dependence on G_d with a constant

$\beta = 0.125$. Figure 10 shows dimensionless inner pressure p_i/G_d versus volume ratio v_c/v_{co}, for different values of G_d, from $G_d = 10^7$ Pa to $G_d = 10^9$ Pa. The solid blue line represent the same case as the solid blue line of figure 9 (with a different scale of the vertical axis); this curve does not intersect the dashed blue line corresponding to the dimensionless cavitation pressure. On the contrary, both the green and orange solid lines, corresponding to higher G_d intersect the cavitation pressure lines (orange and green dashed lines); for $G_d = 10^9$ Pa, cavitation pressure is achieved very soon, for v_c/v_{co} slightly less than 1.

Finally, in figure 11, we present the result of our analyses with a contour plot of the inner pressure in the plane G_d, β; in figure 11 the iso-contour $p_i = -10$ MPa is highlighted by the arrow; such a contour plot may be interpreted as a phase diagram for cavitation to occur. We ran many numerical experiments to explore the space (β, G_d), and for each experiment we evaluated the inner pressure at $v_c/v_{co} = 0.3$, that is, at the maximum achievable value without self contact of hydrogels walls. Based on these pressure values, we interpolated iso–pressure lines; the contour at $p_i = -10$ MPa discriminate between a region where cavitation may occur and a region where it cannot.

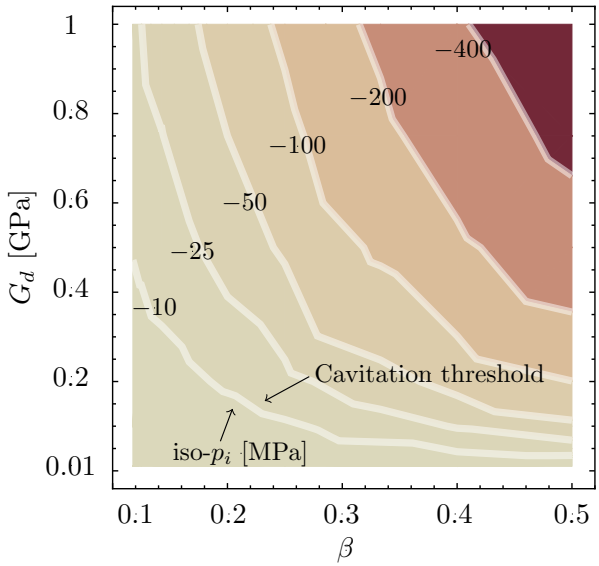

Fig. 11 Phase diagram of cavity pressure. In the plane G_d, β, we highlight the isolines for the inner pressure p_i. The isoline $p_i = -10$ Mpa corresponds to the cavitation threshold: above this line, cavitation may occur. All the values of p_i have been evaluated at $v_c/v_{co} = 0.3$.

6 Dehydration under spherical symmetry

We discuss our ideal experiment, dehydration of a gel with a cavity filled with water, by considering a spherical sample. For a spherical geometry, this problem also allows for an analytical approximation based on the analysis developed in Ref. 20. Therein, the phenomenon of hole formation in the interior of an elastic body in a state of tension has been studied and referred as cavitation, as it was common since the ′80 after the seminal paper by J.M. Ball cited as Ref. 23[§].

When dehydration preserves the condition of spherical symmetry, no inflatable–balloon mode is visible. Nevertheless, at early times, as already observed for the cubic sample, the inner pressure p_i increases, meanwhile the wall thickness decreases. Then, after achieving a maximum positive value, the pressure decreases to negative values, while the walls thicken.

It follows that, also for the spherical geometry, dehydration exhibits two phases, see figure 12. In particular, compare the top panels of figures 3 and 12. These two phases, wall-thinning and wall-thickening, determine the so-called *breathing mode*, a not monotone deformation mode characteristic of cavities filled with water. In this case, the cavity reduces its size but retains the spherical shape[25]. We remark that the same phenomenon, a non monotone change of the wall thickness during dehydration, has been observed in our numerical experiments with cubic samples.

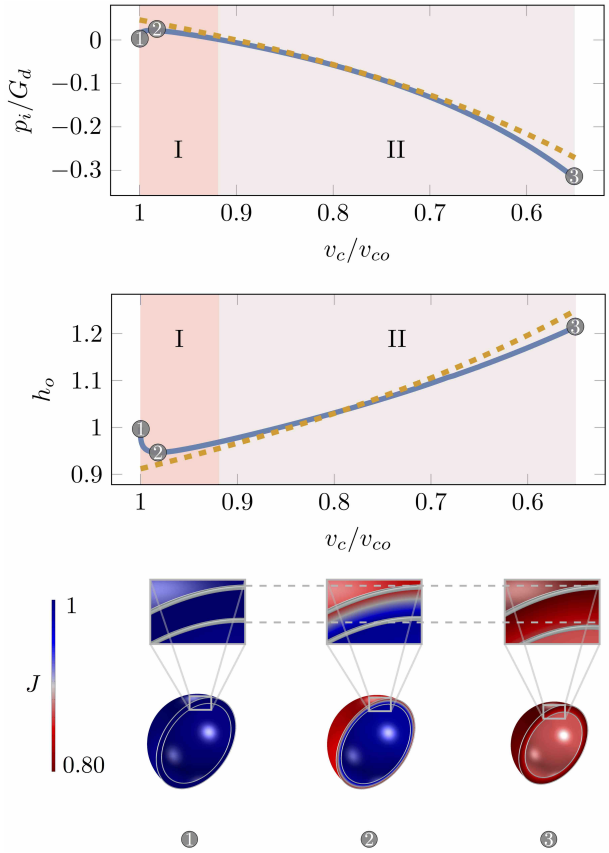

Fig. 12 The breathing mode of a spherical cavity is represented in terms of the dimensionless pressure p_i/G_d (top), and of the dimensionless walls thickness h_o (central panel) versus v_c/v_{co}. Results from an approximate explicit analysis (dashed orange lines) and from numerical solutions (solid blue lines) are compared. The change in volume of the sphere walls is represented through a colour code related to J_d (bottom panel). The geometry of the dry sphere is fixed by the external R_e and internal radius R_c: $R_e = 0.01$m, and $R_c = 0.00875$m.

§ Successively, within the context of solid mechanics, cavitation has also been used as a synonymous for *discontinuous change of size* of an existing cavity in a solid, as in Refs. 21,22,24 which focus on a hydrogel sphere with a cavity.

6.1 The explicit solution

We propose an explicit solution of the dehydration problem by following the solution proposed in Ref. 20. We consider a dry sphere having radius R_e, with a spherical cavity at its center of radius R_c. Under spherical symmetry conditions, the deformation of the sphere is described by the map $r(R)$ which delivers the actual radius r corresponding to the dry one R.

Our numerical experiments show that, both for the cubic and the spherical samples, the gel volume $v_g(t)$ remains constant during dehydration when $t \gg T_c$; we can write:

$$v_g(t)|_{t\gg T_c} \simeq \bar{J}_d\, v_{gd}\,, \quad \text{with}\, v_{gd} = \text{gel volume at dry state.} \quad (6.28)$$

Moreover, the value of $\bar{J}_d$ can be approximated by averaging the values of J_d imposed by the chemical boundary conditions: at $\partial\mathscr{B}_c$ we have $\mu = 0$ J/mol, and $J_d = J_o$; at $\partial_e\mathscr{B}_d$ we have $\mu = \mu_\infty$, and $J_d = 1$; it holds

$$\bar{J}_d = \frac{1+J_o}{2}\,, \quad (6.29)$$

with the value of J_o controlled by the chemical potential through the equation (3.17). Equation (6.29) is the key to solve our problem; introducing the radial stretch λ_R and the hoop stretch λ_ϑ: we can write

$$\bar{J}_d = \lambda_R\,\lambda_\vartheta^2\,, \quad \text{with} \quad \lambda_R(R) = r'(R)\,, \quad \lambda_\vartheta(R) = \frac{r(R)}{R}\,. \quad (6.30)$$

Equations (6.30) yield an ODE that can be integrated explicitly:

$$r'(R)\left(\frac{r(R)}{R}\right)^2 = \bar{J}_d\,; \quad \text{boundary condition } r(R_c) = r_c\,. \quad (6.31)$$

The solution of (6.31) is the function

$$r(R) = (\,r_c^3 + \bar{J}_d\,(R^3 - R_c^3)\,)^{1/3}\,. \quad (6.32)$$

The hoop stretches at cavity and at the external boundary are

$$\lambda_c = \lambda_\vartheta(R_c) = \frac{r_c}{R_c}\,; \quad \lambda_e = \lambda_\vartheta(R_e) = \frac{r(R_e)}{R_e}\,. \quad (6.33)$$

Then, given the elastic energy density per unit reference volume $\hat{W} = \hat{W}(\lambda_R, \lambda_\vartheta)$, the total potential energy of the sphere can be written as:

$$\mathscr{E} = \int_{R_c}^{R_e} 4\,\pi R^2 \hat{W}(\lambda_R, \lambda_\vartheta)\, dR - p_i\, 4\pi R_c^3(\lambda_c - 1)\,, \quad (6.34)$$

Following Ref. 20, we assume a change of variable, $r/R = t$, and consider the elastic energy as a function of t:

$$\hat{W}(\lambda_R, \lambda_\vartheta) = \hat{W}\left(\frac{\bar{J}_d}{\lambda_\vartheta^2}, \lambda_\vartheta\right) = W(t)\,. \quad (6.35)$$

Moreover, from the change of variable, and from (6.32), we have

$$dt = \frac{\bar{J}_d - t^3}{t^2}\,\frac{dR}{R}\,, \quad R^3 = \frac{r_c^3 - \bar{J}_d R_c^3}{t^3 - \bar{J}_d}\,, \quad (6.36)$$

and we can use these relations to rewrite the first summand of (6.37) as an integral over t

$$\int_{R_c}^{R_e} 4\,\pi R^2 \hat{W}(\lambda_R, \lambda_\vartheta)\, dR = 4\,\pi\,(r_c^3 - \bar{J}_d R_c^3)\int_{\lambda_e}^{\lambda_c} \frac{t^2}{(t^3 - J_d)^2}\, W(t)\, dt\,. \quad (6.37)$$

Then, integrating by parts, we obtain:

$$\mathscr{E} = \frac{4\,\pi}{3}\,(r_c^3 - \bar{J}_d R_c^3)\int_{\lambda_e}^{\lambda_c} \frac{W'}{(t^3 - \bar{J}_d)}\, dt + \frac{4\,\pi}{3}\left(R_e^3 W(\lambda_e) - R_c^3 W(\lambda_c)\right) - p_i\, 4\,\pi R_c^3\,(\lambda_c - 1)\,. \quad (6.38)$$

Finally, from the stationary condition we obtain a formula for p_i

$$\frac{d\mathscr{E}}{dr_c} = 0 \quad \Rightarrow \quad p_i = \lambda_c^2 \int_{\lambda_e}^{\lambda_c} \frac{W'}{(t^3 - \bar{J}_d)}\, dt\,. \quad (6.39)$$

For a neo–hookean elastic energy, we have

$$W(t) = \frac{G_d}{2}(\bar{J}_d^2 t^{-4} + 2t^2 - 3)\,. \quad (6.40)$$

Inserting (6.40) in (6.39) yields the inner pressure as a function of G_d, $\bar{J}_d$ (that is, the chemical boundary conditions), and the two hoop stretches λ_c , λ_e:

$$\frac{p_i}{G_d} = \frac{\lambda_c}{2}\left(\frac{\bar{J}_d + 4\,\lambda_e^3}{\lambda_e^4} - \frac{\bar{J}_d + 4\,\lambda_c^3}{\lambda_c^4}\right)\,. \quad (6.41)$$

Actually, $\bar{J}_d$, λ_e, and λ_c are not independent; as example, by using (6.32), we can write λ_e as a function of $\bar{J}_d$ and λ_c

$$\lambda_e = \bar{J}_d + \left(\frac{R_c}{R_e}\right)^3 (\lambda_c^3 - \bar{J}_d)\,. \quad (6.42)$$

It is worth introducing the cavity hoop-stretch $\tilde{\lambda}_c$, as measured with respect to the hoop stretch at the free-swollen state λ_{co}; it is given by

$$\tilde{\lambda}_c = \frac{r_c}{R_{co}} = \frac{\lambda_c}{\lambda_{co}} = \left(\frac{v_c}{v_{co}}\right)^{1/3}\,. \quad (6.43)$$

Thus, using (6.42) and (6.43), it is possible to rewrite (6.41) as a function of the free-swollen stretch of the cavity λ_{co}, and the volume ratio v_c/v_{co}:

$$\frac{p_i}{G_d} = -\frac{1}{2}\left(\frac{v_c}{v_{co}}\right)^{1/3} \frac{\bar{J}_d + 4\,\lambda_{co}^3\,(v_c/v_{co})}{\lambda_{co}^3(v_c/v_{co})}\,\lambda_{co} + \frac{1}{2}\,\frac{5\,\bar{J}_d - 4\,(\bar{J}_d - \lambda_{co}^3\,(v_c/v_{co}))\,(R_c/R_e)^3}{(\bar{J}_d - (\bar{J}_d - \lambda_{co}^3\,(v_c/v_{co}))\,(R_c/R_e)^3)^{4/3}}\,\lambda_{co}^2\,(v_c/v_{co})^{2/3}\,. \quad (6.44)$$

Figure 12, top panel, shows the dimensionless pressure p_i/G_d as evaluated by the explicit formula (6.44) (orange, dashed), and by numerical simulations (blue, solid), for $\lambda_{co} = 1.077$ and $\bar{J}_d = 1.124$. The dimensionless thickness

$$h_o = \frac{r(R_e) - r_c}{(R_e - R_c)\lambda_{co}}\,, \quad (6.45)$$

is an important determinant of the breathing mode: figure 12 (middle) shows the non monotone behavior of h_o versus (v_c/v_{co}).

7 Conclusions

In summary, we have proposed a mathematical model that describes the de–hydration process of a hydrogel with a cavity filled with water and comprehend the modeling of the so–called suction effect. Moreover, we also implemented the model through a commercial finite element software and showed the emergence at early times of a deformative mode which makes the sample similar to an inflatable balloon. The numerics and experiments we carried on underlied the importance of material and geometrical parameters in pursuing water cavitation within the cavity. Finally, we showed as, for spherical samples, the early times deformative mode is a breathing mode.

Conflict of interest

There are no conflicts to declare.

References

1 P. R. Gogate and A. B. Pandit, *AIChE Journal*, 2000, **46**, 1641–1649.

2 A. I. Nesterenko and Y. S. Berlizov, *Chemistry and Technology of Fuels and Oils*, 2007, **43**, 515–518.

3 O. Vincent, P. Marmottant, P. A. Quinto-Su and C.-D. Ohl, *Phys. Rev. Lett.*, 2012, **108**, 184502.

4 X. Noblin, N. O. Rojas, J. Westbrook, C. Llorens, M. Argentina and J. Dumais, *Science*, 2012, **335**, 1322–1322.

5 A. Sakes, M. van der Wiel, P. W. J. Henselmans, J. L. van Leeuwen, D. Dodou and P. Breedveld, *PLOS ONE*, 2016, **11**, 1–46.

6 C. Llorens, M. Argentina, N. Rojas, J. Westbrook, J. Dumais and X. Noblin, *Journal of The Royal Society Interface*, 2016, **13**, –.

7 A. Lucantonio, P. Nardinocchi and L. Teresi, *Journal of the Mechanics and Physics of Solids*, 2013, **61**, 205 – 218.

8 A. Lucantonio, M. Roche, P. Nardinocchi and H. A. Stone, *Soft Matter*, 2014, **10**, 2800–2804.

9 A. Lucantonio, P. Nardinocchi and H. A. Stone, *Journal of Applied Physics*, 2014, **115**, –.

10 M. Curatolo, P. Nardinocchi, E. Puntel and L. Teresi, *Journal of Applied Physics*, 2017, **122**, 145109–1 – 145109–8.

11 W. Hong, X. Zhao, J. Zhou and Z. Suo, *Journal of the Mechanics and Physics of Solids*, 2008, **56**, 1779 – 1793.

12 W. Hong, Z. Liu and Z. Suo, *International Journal of Solids and Structures*, 2009, **46**, 3282 – 3289.

13 J. Zhang, X. Zhao, Z. Suo and H. Jiang, *Journal of Applied Physics*, 2009, **105**, 093522.

14 S. A. Chester and L. Anand, *Journal of the Mechanics and Physics of Solids*, 2010, **58**, 1879 – 1906.

15 P. J. Flory and J. Rehner, *J Chem Phys*, 1943, **11**, 512–520.

16 P. J. Flory and J. Rehner, *J Chem Phys*, 1943, **11**, 521–526.

17 S. Cai and Z. Suo, *Journal of the Mechanics and Physics of Solids*, 2011, **59**, 2259 – 2278.

18 A. D. Drozdov, A. Papadimitriou, J. Liely and C.-G. Sanporean, *Mechanics of Materials*, 2016, **102**, 61–73.

19 E. Cirillo, P. Nardinocchi and G. Sciarra, *International Journal of Non-Linear Mechanics*, 2016, **81**, 115 – 121.

20 S. Biwa, *International Journal of Non-Linear Mechanics*, 2006, **41**, 1084 – 1094.

21 F. P. Duda, A. C. Souza and E. Fried, *Journal of the Mechanics and Physics of Solids*, 2011, **59**, 2341 – 2354.

22 H. Wang and S. Cai, *Soft Matter*, 2015, **11**, 1058–1061.

23 J. M.Ball, *Philosophical Transactions of the Royal Society of London A: Mathematical, Physical and Engineering Sciences*, 1982, **306**, 557–611.

24 H. Wang and S. Cai, *Journal of Applied Physics*, 2015, **117**, 154901.

25 S. Cai, K. Bertoldi, H. Wang and Z. Suo, *Soft Matter*, 2010, **6**, 5770–5777.